The Reaction between Sodium Hydroxide and Atomic Hydrogen in Atmospheric and Flame Chemistry

J. C. Gómez Martín, C. Seaton, M. P. de Miranda and J. M. C Plane*

School of Chemistry, University of Leeds, Woodhouse Lane, LS2 9JT, Leeds, UK

*Correspondence to: J.M.C.Plane@leeds.ac.uk

Abstract

We report the first direct kinetic study of the gas-phase reaction NaOH + H → Na + H_2O, which is central to the chemistry of sodium in the upper atmosphere and in flames. The reaction was studied in a fast flow tube where NaOH was observed by multi-photon ionization and time-of-flight mass spectrometry, yielding k(NaOH + H, 230 - 298 K) = (3.8 ± 0.8) × 10^{-11} cm^3 $molecule^{-1}$ s^{-1} (at 2σ confidence level), showing no significant temperature dependence over the indicated temperature range and essentially in agreement with previous estimates of the rate constant in hydrogen-rich flames. We show, using theoretical trajectory calculations that the unexpectedly slow, yet T-independent, rate coefficient for NaOH + H is explained by severe constraints in the angle of attack that H can make on NaOH to produce H_2O. This reaction is also central to explaining Na-catalyzed flame-inhibition, which has been proposed to occur via the sequence Na + OH (+ M) → NaOH followed by NaOH + H → Na + H_2O, thereby effectively recombinating H and OH to H_2O. RRKM calculations for the recombination of Na and OH yield k(Na + OH + N_2, 300 - 2400 K) = 2.7 × 10^{-29} (300 / T)$^{1.2}$ cm^6 $molecule^{-2}$ s^{-1}, in agreement with a previous flash photolysis measurement at 653 K, and Na-seeded flame studies in the 1800 - 2200 K range. This implies that strong evidence supporting the mechanism of flame inhibition by Na has been stablished.

1. Introduction

Sodium atoms, molecules and ions occur in planetary atmospheres as a result of ablation of the continuous influx of interplanetary dust particles (IDPs) from the Zodiacal Cloud complex.[1] Meteor showers, which result from the interception of fresh cometary trails by the orbit of a planet, also contribute to the formation of Na-rich planetary sporadic layers.[2, 3] A beautiful example of this phenomenon has been recently shown by the MAVEN observations of the Martian atmosphere after being engulfed by the coma of the comet Siding Spring in 2015.[4] The Earth's Na layer, which peaks around 90 km, was the first of the meteoric metallic layers to be observed and studied,[5] and owing to its stability and the ease of observation, has been regularly used as a probe of the chemistry and dynamics of the mesosphere-lower thermosphere region of the Earth's atmosphere.[6-11] Na is also key in the detection of incoming micrometeoroids, because its abundance and low ionisation potential generate high electron densities around the meteor heads, which back-scatter efficiently the radiation beams emitted by high performance radars.[12-14]

We have recently contributed to advances in the understanding of different aspects of the chemistry of Na, such as the mechanism responsible for the D-line ratio variability[15] and the formation of reservoir and sink molecules.[16] Above the Na neutral layer, Na^+ ions are formed by charge transfer of Na with NO^+ and O_2^+ and by photo-ionisation. The formation of ion clusters, followed by dissociative electron recombination, leads to neutralization of Na^+. Below 90 km, Na is converted into less reactive neutral species:

$$Na + O_3 \rightarrow NaO + O_2 \qquad (\Delta H_r = -163.0 \text{ kJ mol}^{-1}) \qquad (R1)$$

$$NaO + H_2O \rightarrow NaOH + OH \qquad (\Delta H_r = +1.4 \text{ kJ mol}^{-1}) \qquad (R2)$$

$$NaO + H_2 \rightarrow NaOH + H \qquad (\Delta H_r = -60.0 \text{ kJ mol}^{-1}) \qquad (R3)$$

$NaOH + CO_2 + M \rightarrow NaHCO_3 + M$ (ΔH_r = -132.0 kJ mol^{-1}) (R4)

We have reported new measurements of the rate constants for R2 - R4 and given recommended values for these rate constants after evaluation of all the literature available.[16] R2 is the most important source of NaOH in the terrestrial atmosphere and $NaHCO_3$ acts as a reservoir species for Na because it is a stable, closed-shell molecule. Besides photolysis and the reaction between sodium bicarbonate and H,[17] there is one additional path back to the reactive species Na and NaO:

$NaOH + H \rightarrow Na + H_2O$ (ΔH_r = -161.7 kJ mol^{-1}) (R5)

Of all the neutral Na reactions considered to be important in the Earth's mesosphere, R5 is the only one for which a rate coefficient at relevant temperatures has not been reported yet. Only a lower limit k_5(308 K) > 4×10^{-12} cm^3 molecule^{-1} s^{-1} has been published.[18] High temperature measurements of k_5 in fuel-rich flames have been also reported, with k_5(1800 – 2200 K) = 1.8×10^{-11} exp(-990/T) cm^3 molecule^{-1} s^{-1}, with a factor of 3 uncertainty in the pre-exponential factor.[19] Extrapolation of this expression to room temperature yields k_5 (300 K) = 6.4×10^{-13} cm^3 molecule^{-1} s^{-1}, although this is not an acceptable practice and in fact the authors of this work acknowledged substantial uncertainty in the temperature dependence of k_5. Another estimate of k_5(1600 – 2400 K) ≤ 0.7×10^{-11} $T^{1/2}$ exp(-1684/T) cm^3 molecule^{-1} s^{-1} was reported from measurements in an oxygen-rich H_2 flame,[20] which extrapolates to k_5(300 K) ≤ 4.4×10^{-12} cm^3 molecule^{-1} s^{-1}. In our previous studies modelling the mesospheric Na layer,[21, 22] the temperature-dependent expression $k_5(T) = 4 \times 10^{-11}$ exp(-550/T) cm^3 molecule^{-1} s^{-1} (T = 200 - 300 K) was used to obtain good agreement between the model and the observed underside of the Na layer. This expression gives k_5(300 K) = 6.4×10^{-12} cm^3 molecule^{-1} s^{-1}, close to the extrapolated upper limit of Hynes, et al. [20]. However, k_2 and k_4 have recently been re-

measured,[16] and we showed that a value of $k_5(200\ K) \sim 5 \times 10^{-11}$ cm^3 molecule^{-1} s^{-1} was necessary to bring the modelled Na layer into agreement with observations. Combining this result with the high temperature flame measurements implies that reaction 5 must have a small temperature dependence.

R5 is also relevant in combustion chemistry studies. The flame-inhibiting property of Na has been known for many decades, and is proposed to occur via the reaction

$$Na + OH + M \rightarrow NaOH + M \qquad (\Delta H_r = -335.4\ kJ\ mol^{-1}) \qquad (R6)$$

followed by R5, which therefore catalyzes the recombination of H and OH to H_2O.[19] The rate coefficient for R6 has been measured directly with M = He at 653 K,[23] and an estimate between 1800 and 2200 K was obtained from flames seeded with Na (M = H_2O, H_2 or N_2.).[19]

In this paper, we present the first direct experimental measurement of R5 by observing the removal of NaOH in the presence of H, as well as formation of the Na product. The unexpectedly slow and temperature-independent rate coefficient is then interpreted using theoretical trajectory calculations. Lastly, the implications for sodium chemistry in the terrestrial mesosphere and for flame inhibition are discussed, including Master equation modelling of R6 to obtain a temperature-dependent expression encompassing the available measurements at different temperatures.

2. Experimental techniques

The reaction was studied in a fast flow tube reactor coupled to a laser induced fluorescence (LIF) and atomic resonance fluorescence (ARF) detection manifold for Na and H respectively. Figure 1 is a schematic drawing of the stainless steel flow tube, which has a total length of 600 mm (Na source to optical detection point) and an inner diameter of 38 mm. In an alternative

arrangement, the flow tube was coupled to a Photo-Ionization Time-of-Flight Mass Spectrometer (PI-ToF-MS) system to detect H and NaOH, with the same configuration used in our previous study.[16]

The reactant NaOH was produced in situ from a series of reactions. Na vapour from a heat-pipe (T = 600 K)[16, 17] was entrained in a flow of N_2 (typically 3 standard litres per minute, slm) carrying 2% N_2O and 0.01% H_2O (or 1% H_2). First, NaO was generated from the reaction of Na with N_2O:

$$Na + N_2O \rightarrow NaO + N_2 \qquad (R7)$$

This was followed by reaction of NaO with H_2O or H_2 (R2 or R3) to make NaOH, which was subsequently reacted with atomic hydrogen (R5) further downstream after R2 or R3 had essentially (> 99.9%) gone to completion. Atomic H was produced by the microwave (MW) discharge (Opthos Instruments model MO-4, Evenson cavity, 120 W, 2.45 GHz) of a flow of H_2 in He and injected through an inlet in a side port 310 mm upstream of the detection point. A large excess of CO was added 6.8 centimetres upstream of the H injection to prevent reformation of NaOH from NaO formed via R5, R7 and R2 or R3:

$$NaO + CO \rightarrow Na + CO_2 \qquad (R8)$$

The relatively large rate constant for this reaction ($k_8 = 9 \times 10^{-11}$ cm^3 molecule^{-1} s^{-1}) was reported in our previous study,[16] and is in reasonable agreement with an earlier study.[24] R5 was studied by changing the flow of H_2 through the microwave, while keeping H in large excess over NaOH (~10^{13} atom cm^{-3} vs. ~10^9 molecule cm^{-3}). The total flow rate through the flow tube was also changed to vary the contact time between the reactants (i.e. the time that the reactants spend well mixed with the carrier gas in the flow tube before reaching the detection point).

Under these conditions, the only reactions to consider are R5 and the diffusive losses of Na, NaOH and H towards the walls:

$Na \rightarrow wall$ (R9)

$NaOH \rightarrow wall$ (R10)

$H \rightarrow wall$ (R11)

Downstream of the oven source, the flow tube was fitted with a six-way cross through which ARF and LIF measurements of key species could be performed. The Ly-α emission from a radiofrequency (RF) discharge on a flow of He (10 sccm, ~1 Torr) containing trace H_2 was directed perpendicular to the flow tube axis; H atom resonance fluorescence was collected orthogonally through an N_2-purged optical path containing a set of baffles and an interference filter (20% peak efficiency at 121.6 nm), and measured using a solar blind photomultiplier (PMT). The RF signal was recorded and averaged continuously by a digital oscilloscope (LeCroy LT342). The H atom relative concentration measurement was used first to determine the wall loss rate of H (R11) by varying the total flow rate and pressure in the flow tube to change the residence time between the injection and detection points, while keeping the flow through the MW discharge constant. A linear-exponential expression is fitted to the data where, besides diffusion to walls, dilution by addition of different carrier gas flows is accounted for. Knowing that the H loss rate may depend on the wall's chemical state, and definitely depends on pressure and temperature, measurements of k_{11}^{wall} were carried out immediately before each determination of k_5. The loss rates derived were consistent with previous determinations in the same system using a movable axial H atom MW injector[17].

The H atom absolute concentration at the H injection point, $[H]_0$, was determined before each NaOH experiment by adding NO_2 ($\sim 5 \times 10^{14}$ molecule cm^{-3}) to the carrier flow and measuring

the fraction removed by the fast reaction [25]:

$NO_2 + H \rightarrow NO + OH$ (R12)

NO_2 was monitored by LIF [26] at 592 nm using a frequency-doubled Nd:YAG laser (Continuum Surelite 10-II) to pump a dye laser (Sirah Cobra Stretch) with Rhodamine 610 dye. The excitation beam passed through the six-way crossing perpendicular to the flow and the resulting non-resonant NO_2 fluorescence was measured orthogonally through a 610 nm long-pass filter with a PMT. The LIF decay signal was then captured by the second channel of the digital scope and integrated by setting up a gate around the LIF signal decay (excluding the small laser scatter peak, which is ~10 ns in width) with the scope built-in boxcar function. Typically, at least 100 laser shots were accumulated before the concentration of H was changed. When the MW discharge was on, the NO_2 LIF signal dropped because of the stoichiometric reaction between NO_2 and H (R12). Thus, $[H]_0$ was equal to the observed loss of NO_2 ($[H]_0 = -\Delta[NO_2]$), with the initial $[NO_2]$ derived from manometric and flowmeter readings. The error due to recycling of H from the products of NO_2 + H or by third-order removal of NO_2 was calculated to be smaller than 5% by numerical modelling using evaluated rate constants.[25] The relative H concentration at the RF detection point was found to vary linearly with $[H]_0$, which was changed by varying the H_2 flow through the MW discharge, and therefore could be scaled to $[H]_0$. Note that this calibration is only valid for a given set of temperature, pressure and flow rate conditions, since these determine the wall losses of H between injection and detection and therefore the detected signal. Calibrations were therefore performed under different conditions of flow and pressure (an example is shown in the insert of Figure 2).

After the H calibration, the same laser used to monitor NO_2 was tuned to the $3^2P_{3/2} \leftarrow 3^2S_{1/2}$ transition of Na at 588.99 nm, and the resulting LIF signal was collected perpendicularly by a PMT through a narrow band interference filter (FWHM = 5 nm) and a set of lenses. The wall

loss rate of Na, k_9^{wall}, was measured by varying the residence time of the gas mixture in the flow tube in the absence of reactants. During the main experiments, Na LIF was used to monitor the relative concentration of Na generated as a function of $[H]_0$.

An additional set of experiments was carried where NaOH was measured by PI-ToF-MS.[16] Briefly, the six-way crossing in Fig. 2 was replaced by a CF flange interface to the PI-ToF-MS. The gas in the flow tube was sampled on-axis from the core of the laminar flow via a skimmer cone with a 200 μm pinhole. NaOH was photo-ionised using a laser at 315 nm (2-photon ionisation) and detected at m/z = 40. In these experiments R12 was also used to determine the H concentration at the injection point. NO_2 was ionized by electron impact at 70 eV and detected by the ToF-MS at m/z = 46. The H atom wall loss rate k_{11}^{wall} was measured for each determination of k_5 by injecting NO_2 at different distances downstream of the microwave discharge, plotting the resulting $\Delta[NO_2]$ vs the equivalent flight times between the MW discharge and the NO_2 injection point, and fitting a single exponential decay to the data.

Gases, reactants and sodium metal were handled as described previously.[16] The reactant flows (N_2O, H_2, H_2O, CO, NO_2) were set with calibrated mass flow controllers (MKS Instruments). The pressure and temperature at the oven and in the flow tube were measured using calibrated capacitance manometers (Baratron) and T-type thermocouples (Omega), respectively. The pressure was maintained in the 0.5-3 Torr range. Due to the relatively low temperature needed in the Na oven to generate detectable LIF Na signals (~10^9 atom cm^{-3}), the reaction zone never went above room temperature. Under these conditions, the Reynolds number was maintained in the 50-200 range, i.e. within the laminar flow regime, so that the well-established parabolic flow velocity correction could be applied.[16] Experiments were also carried out at low temperature (230 K) by packing chips of solid CO_2 around the flow tube and the carrier gas supply line.

4. Experimental results

The removal of NaOH and simultaneous re-appearance of Na upon addition of H atoms through the MW discharge port can be described by the following set of coupled differential equations:

$$\frac{d[\mathrm{Na}]}{dt} = k_5[\mathrm{H}][\mathrm{NaOH}] - k_9^{\mathrm{wall}}[\mathrm{Na}] \qquad \text{(E1)}$$

$$\frac{d[\mathrm{NaOH}]}{dt} = -k_5[\mathrm{H}][\mathrm{NaOH}] - k_{10}^{\mathrm{wall}}[\mathrm{NaOH}] \qquad \text{(E2)}$$

$$\frac{d[\mathrm{H}]}{dt} = -k_5[\mathrm{H}][\mathrm{NaOH}] - k_{11}^{\mathrm{wall}}[\mathrm{H}] \sim -k_{11}^{\mathrm{wall}}[\mathrm{H}] \qquad \text{(E3)}$$

This system is solvable analytically for NaOH, but not Na, due to the complex exponential dependence of [NaOH] on t:

$$[\mathrm{NaOH}]=[\mathrm{NaOH}]_0 \exp\left\{-\left[1 - \exp\left(-k_{11}^{\mathrm{wall}}t\right)\right]\frac{k_5[\mathrm{H}]_0}{-k_{11}^{\mathrm{wall}}} - k_{10}^{\mathrm{wall}}t\right\} = A \exp\left(-B[\mathrm{H}]_0\right) \qquad \text{(E4)}$$

where $A = [\mathrm{NaOH}]_0 \exp\left(-k_{10}^{\mathrm{wall}}t\right)$ and $B = \left[1 - \exp\left(-k_{11}^{\mathrm{wall}}t\right)\right] k_5 \left(k_{11}^{\mathrm{wall}}\right)^{-1}$. Inserting E4 in E1 results in a differential equation with nested exponential dependences on t, which cannot be solved analytically without making crude simplifications. Instead, in order to model the Na experimental data and derive k_5, a numerical solution to the reaction scheme including all reactions in the flow tube (R2-R10) was used. The model was numerically integrated to generate concentration vs. time curves of the different species. Simulations for each $[\mathrm{H}]_0$ (i.e. [H] at the injection point) were run between injection of Na (time zero) and arrival at the sampling point (residence time t), with injections of CO and H at specific times calculated by dividing the injection distance to the sampling point over the linear speed of the flow, and applying the parabolic velocity profile correction factor of 1.6.[27] An example of a simulation is shown in Figure 1. The last point of each concentration vs. time simulation was retained and the simulated H-dependent behaviour of Na at the time t (e.g. 25 ms in Figure 1) was then fitted

to the observed data using a nonlinear least-squares routine with k_5 as a floating parameter. Typical examples of observed and modelled [Na] vs $[H]_0$ are shown in Figure 2. The propagation of uncertainties from the rate coefficients of the reactions in the model to the floating parameter of the fit was achieved by Monte Carlo sampling (sample size = 1000 simulations), where the reference rate coefficients (Table 1) and the wall loss rates measured in the preparative experiments were varied using a uniform random distribution within their associated uncertainty ranges. The estimated uncertainties of the Na and H loss rates using the ARF set-up are of the order of 25%.

Examples of the decay of [NaOH] with increasing $[H]_0$ measured with the ToF-Ms system are shown in Figure 3. In this case the analytical solution of the system of differential equations is given by E4. Therefore, the NaOH decays are fit to equation E4 using a least squares routine. From the fitted parameter B, the rate constant of R5 is given by:

$$k_5 = \left[1 - \exp\left(- k_{11}^{\text{wall}} t\right)\right]^{-1} k_{11}^{\text{wall}} B \qquad \text{(E5)}$$

In the ToF-MS system k_{11}^{wall} values are determined from exponential fits of the decay of [H] as a function of contact time (NO_2 injection distance). The uncertainty in the determination of k_5 using this method are propagated in quadrature from the uncertainty of k_{11}^{wall} (~15%) and of B (~25%) from the parameter error of the corresponding least-squares fits. The rate constants obtained from different experiments are listed in Table 1. The 1σ uncertainties reported in Table 1 for each measurement of k_5 encompass the corresponding errors in the H atom calibration (15-25%), H wall loss rate (15%), reference rate constants employed in the numerical model (10%), and residence time (5%). One measurement of k_5 was carried out at (230 ± 7) K, showing within uncertainty the same value as at room temperature. Figure 3 shows that the rate of decay of [NaOH] is the same at 298 K and 230 K after correction for different

contact times and wall loss rates. The temperature dependence of k_5 is therefore small. A weighted average value in the temperature range 230 K - 298 K of $k_5 = (3.8 \pm 0.8) \times 10^{-11}$ cm^3 molecule^{-1} s^{-1} is recommended. The quoted uncertainty is given at the 2σ confidence level and is calculated from the weighted mean standard deviation.

5. Discussion

The measured value of $k_5 = (3.8 \pm 0.8) \times 10^{-11}$ cm^3 molecule^{-1} s^{-1} reported in the present study between 230 K and 298 K is close to the measurement in a fuel-rich flame of $k_5(2000\ K) = 1.1 \times 10^{-11}$ cm^3 molecule^{-1} s^{-1} with an uncertainty of a factor of 3,[19] and an upper limit of $k_5(2000\ K) \leq 1.3 \times 10^{-10}$ cm^3 molecule^{-1} s^{-1} in a fuel-rich flame.[20] This implies that R5 has a very small temperature dependence. The rate coefficient is also well below the capture rate coefficient, $k_{capture}$, which can be estimated using the approach of Georgievskii and Klippenstein.[28] The parameters needed are: for NaOH, the dipole moment (6.9 D) and "exact" polarizability (2.64×10^{-24} cm^3) calculated at the MP2-B3LYP/6-311+G(2d,p)level of theory using analytic third derivatives, and the ionization potential (7.87 eV) [29]; for H, the polarizability (8.77×10^{-26} cm^3) and ionization potential (13.6 eV) [30]. Application of the standard expressions[28] yields a dipole-induced dipole capture rate coefficient of 7.6×10^{-10} cm^3 molecule^{-1} s^{-1}, and a dispersion capture rate coefficient of 5.5×10^{-10} cm^3 molecule^{-1} s^{-1}. The combined capture rate coefficient, which to a good approximation is 1.3 times the larger of these two,[28] is then $k_{capture} = 9.9 \times 10^{-10}$ cm^3 molecule^{-1} s^{-1} i.e. a factor ~27 times faster than k_5.

5.1 The Reaction Potential Energy Surface and Trajectory Calculations

We now investigate theoretically why R5 has such a small temperature dependence, yet is more than an order of magnitude slower than the capture rate coefficient between NaOH and H. Figure 4 illustrates the potential energy surface (PES) for R5 for co-planar collisions of H with

NaOH (whose geometry is frozen at the MP2/6-311+G(2d,p) level). The surface was calculated using the MP2/6-311+G(2d,p) level of theory, where the Møller-Plesset correlation energy correction takes account of the switch from the ionic nature of the surface in the entrance channel to the covalent exit channel when the H_2O has formed i.e. the charge transfer from Na^+–OH^-–H to Na – OH_2. We have found in previous work on metal atom reactions with fluorinated species,[31] where a similar consideration applies, that this level of theory seems to work satisfactorily. At each point on the PES a new initial guess for the Hartree-Fock wave function was generated. The calculations were performed using the Gaussian 09 suite of programs.[32]

Inspection of the PES shows that there is a restricted side-on geometry for collisions where the H atom can approach close enough to the NaOH molecule to initiate a successful reaction. Head-on collisions at either end of the NaOH are strongly repulsive. Since there is no barrier to side-on collisions, the lack of a significant T-dependence in k_5 is explained. Furthermore, the strong dipole-induced dipole interaction caused by the large dipole moment of NaOH will tend to steer the reactants into head-on collisions, thus further reducing the probability of successful reaction.

We used classical trajectory simulations to obtain insight into the NaOH + H collision dynamics, as well as a theoretical estimate of the reaction rate coefficient. The simulations were carried out using the Born-Oppenheimer Molecular Dynamics (BOMD) method[33, 34] at the MP2-B3LYP/6-311+g(2d,p) level of theory.[32] Trajectories were run at a single collision energy of k_BT at T = 300 K, and with NaOH initially at its linear equilibrium geometry (r_{NaO} = 1.975 Å; r_{OH} = 0.957 Å). These trajectory calculations are described in detail in the Electronic Supplementary Information, including animations of selected trajectories. Two interesting features emerge. First, in the case of unreactive collisions, which were initiated with a large range of starting geometries, H-atom exchange was never observed. Second, reactive collisions

tend to produce a highly vibrationally excited Na-H_2O complex that can be very long-lived, with the time between complex formation and dissociation into Na + H_2O being as long as a few picoseconds (see animation M2 in the ESI).

The reaction cross section at this fixed collision energy (2.5 kJ mol^{-1}) was determined for a fixed angle of approach between the H and NaOH axis. This shows that for collisions at 45º, 90º and 135º to the H-O-Na axis), the reaction cross section is 9.7, 14.7 and 12.3 $Å^2$, respectively; and close to zero for near head-on collisions. The cross section averaged over all angles is then ~7 $Å^2$. Approximating the rate coefficient as the product of the cross section and the mean collision velocity yields an estimate of $k_5 = 1.5 \times 10^{-10}$ cm^3 $molecule^{-1}$ s^{-1}. This value, which is a factor of 4 times larger than the measured value in the present study, is probably an upper limit because the long-range dipole-induced dipole force promotes head-on collisions, which then tend to be unsuccessful because of the short-range repulsion (Figure 4)..

5.2 Atmospheric Implications

We recently reported that k_2(NaO + H_2O) and k_4(NaOH + CO_2) were significantly faster than previous measurements.[16] This impacts on the underside of the mesospheric Na layer because Na is then converted more efficiently into the $NaHCO_3$ reservoir species, causing the modelled peak to be ~2 km higher than observed. Reaction 5 slows down the formation of $NaHCO_3$ via R4 by converting the NaOH intermediate back to Na. In Figure 12 of Gómez Martín, et al. [16] we showed that if k_5 were $\sim 5 \times 10^{-11}$ cm^3 $molecule^{-1}$ s^{-1} (i.e. a factor of 20 times larger than assumed in Na atmospheric chemistry modeling [22]) then the underside and peak height of the layer could be modelled correctly. The value of k_5 measured in the present study confirms that R5 is indeed fast enough, which indicates that the gas-phase chemistry of Na in the mesosphere is now largely understood.

5.3 Implications for flame inhibition

As discussed in the Introduction, Jensen and Jones [19] were able to model the observed Na-catalyzed flame inhibition with k_5(NaOH + H) = 1.1×10^{-11} cm^3 $molecule^{-1}$ s^{-1} and k_6(Na + OH + M) = 2.5×10^{-30} cm^6 $molecule^{-2}$ s^{-1} at 2000 K. However, these rate coefficients were obtained by fitting a coupled set of reactions in a flame model, and thus do not independently validate the underlying mechanism. In the present study we have shown that k_5 is essentially temperature independent between 230 and 298 K, and is close to the flame result at 2000 K (which has a factor of 3 uncertainty).

The only direct kinetic study of R6 is by Husain, et al. [23] who obtained $k_6 = 1.1 \times 10^{-30}$ cm^6 $molecule^{-2}$ s^{-1} at 653 K in He bath gas. We now apply Rice-Ramsperger-Kassel-Markus (RRKM) theory to extrapolate this result to 2000 K and M = N_2, in order to test the flame inhibition mechanism. A solution of the Master Equation (ME) based on the inverse Laplace transform method was used.[35] The internal energies of the NaOH adduct were divided into a contiguous set of grains (width 50 cm^{-1}) containing a bundle of rovibrational states. Each grain was then assigned a set of microcanonical rate coefficients for dissociation, which were determined using inverse Laplace transformation to link them directly to $k_{rec,\infty}$, the high pressure limiting rate coefficient. $k_{rec,\infty}$ was set to 9.4×10^{-10} $(T / 300\ K)^{1/6}$ cm^3 $molecule^{-1}$ s^{-1}, the capture rate coefficient between Na and OH which is principally governed by the dispersion force.[28] The density of states of the adduct was calculated using the Beyer–Swinehart algorithm for the vibrational modes (without making a correction for anharmonicity), and a classical densities of states treatment for the rotational modes.[36] The NaOH bond energy (330 kJ mol^{-1}), vibrational frequencies (275 (×2), 591 and 3951 cm^{-1}) and rotational constant (12.74 GHz) were taken from a high level ab initio study.[29]

The probability of collisional transfer between grains was estimated using the exponential down model, where the average energy for downward transitions is designated $\langle \Delta E \rangle_{down}$.[36] The collision frequencies between NaOH and N_2 or He are dominated by the dipole-induced dipole interaction, and are 6.1×10^{-10} and 5.1×10^{-10} cm^3 $molecule^{-1}$ s^{-1}, respectively.[28] Values of $\langle \Delta E \rangle_{down}$ at 300 K of 80 cm^{-1} for He and 350 cm^{-1} for N_2, which are within the expected range for these third bodies along with a $T^{1/2}$ temperature dependence for $\langle \Delta E \rangle_{down}$,[36, 37] produce satisfactory fits within error to both the direct measurement at 653 K [23] and the flame estimate around 2000 K.[19] These fits are illustrated in Figure 5. The resulting temperature-dependent rate coefficients are k_6(300 - 2400 K, M = He) = 3.8×10^{-30} $(298 \text{ K}/ T)^{1.62}$ cm^6 $molecule^{-2}$ s^{-1} and k_6(300 - 2400 K, M = N_2) = 2.4×10^{-29} $(298 \text{ K}/ T)^{1.26}$ cm^6 $molecule^{-2}$ s^{-1}.

Since the flame estimates of k_5 and k_6 are therefore consistent with the direct kinetic measurements of the present study and Husain, et al. [23] respectively, the Na-catalyzed flame inhibition mechanism proposed by Jensen and Jones [19] appears to be confirmed.

6. Conclusions

We have reported the first experimental study of the reaction between NaOH and H under atmospherically relevant conditions. We have found the rate constant to be $k_5 = (3.8 \pm 0.8) \times 10^{-11}$ cm^3 $molecule^{-1}$ s^{-1}, showing no temperature dependence in the 230 K - 298 K range, and essentially in agreement, within uncertainty, with previous measurements in hydrogen-rich flames. We have shown using theoretical trajectory calculations that the unexpectedly slow, yet T-independent, rate coefficient for NaOH + H is explained by severe constraints in the angle of attack that H can make on NaOH to produce H_2O.

The flame-inhibiting properties of Na have been thought to occur via Na + OH (+ M) $\rightarrow$ NaOH followed by NaOH + H $\rightarrow$ Na + H_2O, which catalyzes the recombination of H and OH

to H_2O. We have carried out RRKM calculations which yield a rate coefficient of k_6 in agreement with a previous direct measurement at 653 K and an estimate obtained from a flame study between 1800 and 2200 K. This implies that strong evidence supporting the mechanism for flame inhibition by Na has been stablished.

Acknowledgments

This study was supported by project number 291332 (CODITA – Cosmic Dust in the Terrestrial Atmosphere) from the European Research Council. Pictures included in the graphical abstract: Left: Bunsen burner, by Arthur Jan Fijałkowski (own work) [GFDL (http://www.gnu.org/copyleft/fdl.html) or CC-BY-SA-3.0 (http://creativecommons.org/licenses/by-sa/3.0/)], via Wikimedia Commons; Right: Looking Down on a Shooting Star, astronaut photo ISS028-E-24847 (https://eol.jsc.nasa.gov/SearchPhotos/photo.pl?mission=ISS028&roll=E&frame=24847), source: Earth Science and Remote Sensing Unit, NASA Johnson Space Center.

Supplementary information: Description of classical trajectory simulations employed to gain insight into the NaOH + H collision dynamics. Two animations of interesting reactive trajectories are included.

References

(1) Nesvorný, D.; Jenniskens, P.; Levison, H. F.; Bottke, W. F.; Vokrouhlický, D.; Gounelle, M., Cometary Origin of the Zodiacal Cloud and Carbonaceous Micrometeorites. Implications for Hot Debris Disks. Astrophys. J. **2010,** 713 (2), 816.

(2) Meister, J.; Eberhardt, P.; Herrmann, U.; Kopp, E.; Hidalgo, M. A.; Sechrist Jr., C. F., D-region Ion Composition During the Winter Anomaly Campaign on January 8, 1977. Space Res. XVIII **1978**, 155-159.

(3) Trigo-Rodriguez, J. M.; Llorca, J., On the Sodium Overabundance in Cometary Meteoroids. Adv. Space Res. **2007,** 39 (4), 517-525.

(4) Benna, M.; Mahaffy, P. R.; Grebowsky, J. M.; Plane, J. M. C.; Yelle, R. V.; Jakosky, B. M., Metallic Ions in the Upper Atmosphere of Mars from the Passage of Comet C/2013 A1 (Siding Spring). Geophys. Res. Lett. **2015,** 42 (12), 4670-4675.

(5) Chapman, S., Notes on Atmospheric Sodium. Astrophys. J. **1939,** 90, 309-316.

(6) Batista, P. P.; Clemesha, B. R.; Simonich, D. M.; Kirchhoff, V. W. J. H., Tidal Oscillations in the Atmospheric Sodium Layer. J. Geophys. Res. **1985,** 90 (D2), 3881-3888.

(7) Clemesha, B. R.; Batista, P. P.; Simonich, D. M., Long-term and Solar Cycle Changes in the Atmospheric Sodium Layer. J. Atmos. Solar-Terr. Phys. **1997,** 59 (13), 1673-1678.

(8) Clemesha, B. R.; Simonich, D. M.; Batista, P. P., A Long-term Trend in the Height of the Atmospheric Sodium Layer: Possible Evidence for Global Change. Geophys. Res. Lett. **1992,** 19 (5), 457-460.

(9) Gardner, C. S.; Liu, A. Z., Chemical Transport of Neutral Atmospheric Constituents by Waves and Turbulence: Theory and Observations. J. Geophys. Res. **2016**, 494–520.

(10) Gardner, C. S.; Voelz, D. G., Lidar Studies of the Nighttime Sodium Layer over Urbana, Illinois: 2. Gravity Waves. J. Geophys. Res. **1987,** 92 (A5), 4673-4694.

(11) Rowlett, J. R.; Gardner, C. S.; Richter, E. S.; Sechrist, C. F., Lidar Observations of Wave-like Structure in the Atmospheric Sodium Layer. Geophys. Res. Lett. **1978,** 5 (8), 683-686.

(12) Janches, D.; Dyrud, L. P.; Broadley, S. L.; Plane, J. M. C., First Observation of Micrometeoroid Differential Ablation in the Atmosphere. Geophys. Res. Lett. **2009,** 36 (6), L06101.

(13) Janches, D.; Plane, J. M. C.; Nesvorný, D.; Feng, W.; Vokrouhlický, D.; Nicolls, M. J., Radar Detectability Studies of Slow and Small Zodiacal Dust Cloud Particles. I. The Case of Arecibo 430 MHz Meteor Head Echo Observations. Astrophys. J. **2014,** 796 (1), 41.

(14) Janches, D.; Swarnalingam, N.; Carrillo-Sanchez, J. D.; Gómez Martín, J. C.; Marshall, R.; Nesvorny, D.; Plane, J. M. C.; W., F.; Pokorny, P., Radar detectability studies of slow and small Zodiacal Dust Cloud Particles: III. The role of sodium and the Head Echo size on the probability of detection. Astrophys. J. **2017,** 843, 1-11.

(15) Plane, J. M. C.; Oetjen, H.; De Miranda, M.; Saiz-Lopez, A.; Gausa, M.; Williams, B., On the Sodium D Line Emission in the Terrestrial Nightglow. J. Atmos. Solar-Terr. Phys. **2012,** 74 (0), 181-188.

(16) Gómez Martín, J. C.; Garraway, S. A.; Plane, J. M. C., Reaction Kinetics of Meteoric Sodium Reservoirs in the Upper Atmosphere. J. Phys. Chem. A **2016,** 120 (9), 1330–1346.

(17) Cox, R. M.; Self, D. E.; Plane, J. M. C., A Study of the Reaction Between $NaHCO_3$ and H: Apparent Closure on the Chemistry of Mesospheric Na. J. Geophys. Res. **2001,** 106 (D2), 1733-1739.

(18) Silver, J. A.; Stanton, A. C.; Zahniser, M. S.; Kolb, C. E., Gas-Phase Reaction Rate of Sodium Hydroxide with Hydrochloric Acid. J. Phys. Chem. **1984,** 88 (14), 3123-3129.

(19) Jensen, D. E.; Jones, G. A., Kinetics of Flame Inhibition by Sodium. J. Chem. Soc., Faraday Trans. 1 **1982,** 78 (9), 2843-2850.

(20) Hynes, A. J.; Steinberg, M.; Schofield, K., The Chemical Kinetics and Thermodynamics of Sodium Species in Oxygen-rich Hydrogen Flames. J. Chem. Phys. **1984,** 80 (6), 2585-2597.

(21) Marsh, D. R.; Janches, D.; Feng, W.; Plane, J. M. C., A Global Model of Meteoric Sodium. J. Geophys. Res. **2013,** 118 (19), 11,442-11,452.

(22) Plane, J. M. C., A Time-resolved Model of the Mesospheric Na Layer: Constraints on the Meteor Input Function. Atmos. Chem. Phys. **2004,** 4, 627-638.

(23) Husain, D.; Plane, J. M. C.; Xiang, C. C., Determination of the Absolute Third-order Rate Constant for the Reaction between Na + OH + He by Time-resolved Molecular Resonance-fluorescence Spectroscopy, OH($A^2\Sigma^+$-$X^2\Pi$), Coupled with Steady Atomic Fluorescence Spectroscopy, Na($3\,^2P$- $3^2S_{1/2}$). J. Chem. Soc., Faraday Trans. 2 **1984,** 80 (12), 1619-1631.

(24) Kolb, C. E.; Worsnop, D. R.; Zahniser, M. S.; Robinson, G. N.; Shi, X.; Herschbach, D. R., Chemical Kinetics and Dynamics of the Mesospheric Sodium Nightglow In Gas Phase Metal Reactions, Fontijn, A., Ed. Elsevier: Amsterdam, 1992; pp 15-27.

(25) Sander, S. P.; Abbatt, J.; Barker, J. R.; Burkholder, J. B.; Friedl, R. R.; Golden, D. M.; Huie, R. E.; Kolb, C. E.; Kurylo, M. J.; Moortgat, G. K., et al. Chemical Kinetics and Photochemical Data for Use in Atmospheric Studies, Evaluation No. 17," JPL Publication 10-6; Jet Propulsion Laboratory: Pasadena, 2011; http://jpldataeval.jpl.nasa.gov.

(26) Thornton, J. A.; Wooldridge, P. J.; Cohen, R. C., Atmospheric NO_2: In Situ Laser-Induced Fluorescence Detection at Parts per Trillion Mixing Ratios. Anal. Chem. **2000,** 72 (3), 528-539.

(27) Brown, R. L., Tubular Flow Reactors with 1st-Order Kinetics. J. Res. Natl. Bur. Stand. **1978,** 83 (1), 1.

(28) Georgievskii, Y.; Klippenstein, S. J., Long-Range Transition State Theory. J. Chem. Phys. **2005,** 122 (19), 194103.

(29) Lee, E. P. F.; Wright, T. G., Heats of Formation of NaOH and $NaOH^+$: Ionization Energy of NaOH. J. Phys. Chem. A **2002,** 106 (38), 8903-8907.

(30) Lide, D. R., Handbook of Physics and Chemistry. CRC Press: Boca Raton, FL, 2006; Vol. 87th. edn.

(31) Totterdill, A.; Gomez Martin, J. C.; Kovacs, T.; Feng, W.; Plane, J. M. C., Experimental Study of the Mesospheric Removal of NF_3 by Neutral Meteoric Metals and Lyman-α Radiation. J. Phys. Chem. A **2014,** 118, 4120-4129.

(32) Frisch, M. J.; Trucks, G. W.; Schlegel, H. B.; Scuseria, G. E.; Robb, M. A.; Cheeseman, J. R.; Scalmani, G.; Barone, V.; Petersson, G. A.; Nakatsuji, H., et al., Gaussian 09, Revision A. 01, Gaussian. Inc., Wallingford, CT **2009**.

(33) Helgaker, T.; Uggerud, E.; Jensen, H. J. A., Integration of the Classical Equations of Motion on ab initio Molecular-Potential Energy Surfaces Using Gradients and Hessians – Application to Translational Energy-Release Upon Fragmentation. Chem. Phys. Lett. **1990,** 173, 145-50.

(34) Li, X.; Millam, J. M.; Schlegel, H. B., Ab Initio Molecular Dynamics Studies of the Photodissociation of Formaldehyde, $H_2CO \rightarrow H_2 + CO$: Direct Classical Trajectory Calculations by MP2 and Density Functional Theory. J. Chem. Phys. **2000,** 113, 10062-10067.

(35) De Avillez Pereira, R.; Baulch, D. L.; Pilling, M. J.; Robertson, S. H.; Zeng, G., Temperature and Pressure Dependence of the Multichannel Rate Coefficients for the CH_3 + OH System. J. Phys. Chem. A **1997,** 101 (50), 9681-9693.

(36) Gilbert, R. G.; Smith, S. C., Theory of Unimolecular and Recombination Reactions. Blackwell: Oxford, 1990.

(37) Glowacki, D. R.; Liang, C.-H.; Morley, C.; Pilling, M. J.; Robertson, S. H., MESMER: An Open-Source Master Equation Solver for Multi-Energy Well Reactions. J. Phys. Chem. A **2012,** 116 (38), 9545-9560.

Tables

Table 1. Rate coefficients and wall loss rates employed in the numerical model used to simulate the formation of Na as a function of $[H]_0$

	Reaction	Rate coefficient /cm^3 molecule^{-1} s^{-1} or loss rate [a] /s^{-1}	Reference
R2	$NaO + H_2O \rightarrow NaOH + OH$	$(2.4 \pm 0.7) \times 10^{-10}$	16
R5	$NaOH + H \rightarrow Na + H_2O$	floated	This work
R7	$Na + N_2O \rightarrow NaO + O_2$	$(1.3 \pm 0.2) \times 10^{-12}$	25
R8	$NaO + CO \rightarrow Na + CO_2$	$(1.2 \pm 0.4) \times 10^{-11}$	16
R9	$Na \rightarrow$ wall	Measured: 180 ± 40	This work
R10	$NaOH \rightarrow$ wall	Assumed to be the same as for R9 [b]	This work
R11	$H \rightarrow$ wall	Measured: 300 ± 80	This work

[a] Rate coefficients at 298 K; Loss rates at 298 K and 1 Torr. Uncertainties at 95% confidence level.

[b] According to measurements by Cox et al.[17] with a similar set-up, k_{10}^{wall}/k_9^{wall}=1.13, which means that k_{10}^{wall} is within the error bar of k_9^{wall}.

Table 2. Determinations of k_5 with corresponding experimental conditions.

Detection	Flow /slm	T /K	P /Torr	t /ms [a]	k_5 /10^{-11} [b]
Na LIF	3.6	298	1.6	7.2	3.8 ± 1.1
	2.4	298	1.6	10.7	4.2 ± 1.2
	3.6	298	3.0	13.5	4.9 ± 1.5
	1.7	298	1.6	15.5	2.0 ± 1.1
	3.1	298	2.0	10.2	4.1 ± 1.9
	3.1	298	1.0	4.9	6.2 ± 2.9
	2.3	298	1.5	10.4	4.0 ± 1.9
	2.6	298	2.0	10.2	5.8 ± 2.6
	5.0	298	1.0	3.2	3.5 ± 1.7
	2.8	298	1.0	5.7	3.2 ± 1.5
NaOH PI-ToF-MS	3.8	298	1.7	5.9	4.1 ± 1.1
	3.8	298	1.7	5.9	3.5 ± 0.8
	5.0	230	2.0	6.7	4.3 ± 1.5
Weighted average					3.8 ± 0.4

[a] Contact time between H and NaOH, i.e. flight time from the MW discharge port to the detection region [b] Rate constant in cm^3 molecule^{-1} s^{-1}. Uncertainty at 1σ confidence level.

Figures

Figure 1

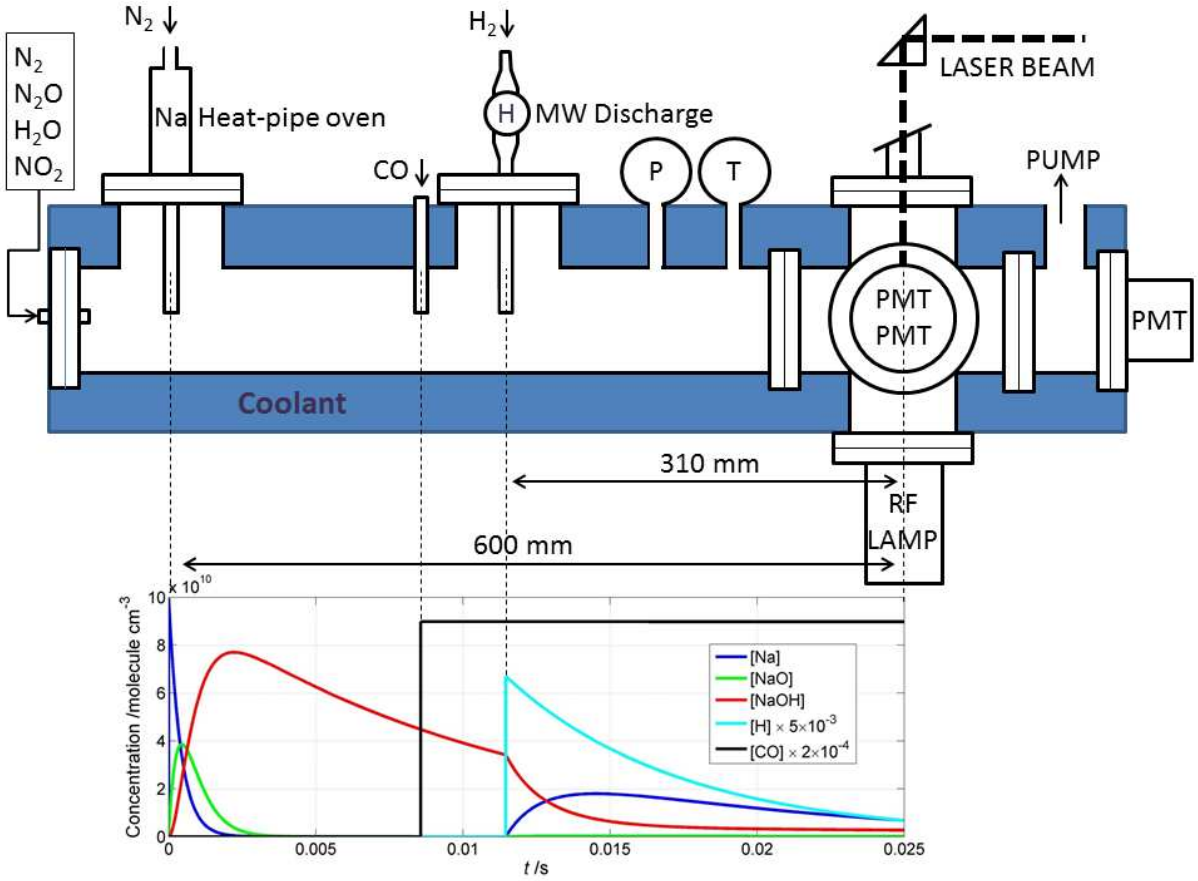

Figure 1 Schematic of the fast flow tube- laser induced fluorescence set-up. Modelled concentrations as a function of residence time (with respect to the Na injection time) of the chemistry occurring in the different sections are shown below.

Figure 2

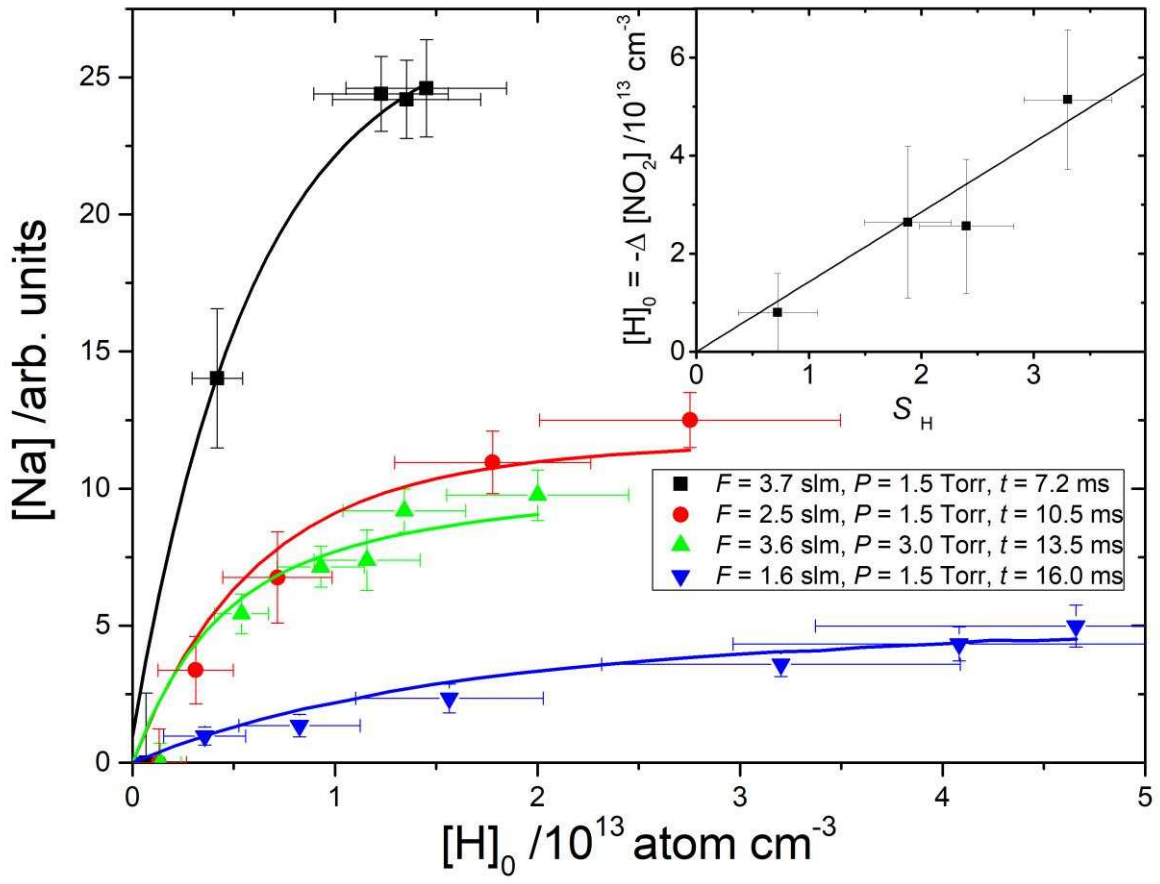

Figure 2. Typical examples of Na growth (concentration in arbitrary units) observed with the LIF system upon addition of increasing H concentration. Flow, pressure and contact time are indicated in the legend. The insert shows the calibration plot (for t = 10.5 ms) of NO_2 removal vs H fluorescence signal (S_H). $[H]_0$ indicates the H atom concentration at the MW discharge injection point.

Figure 3.

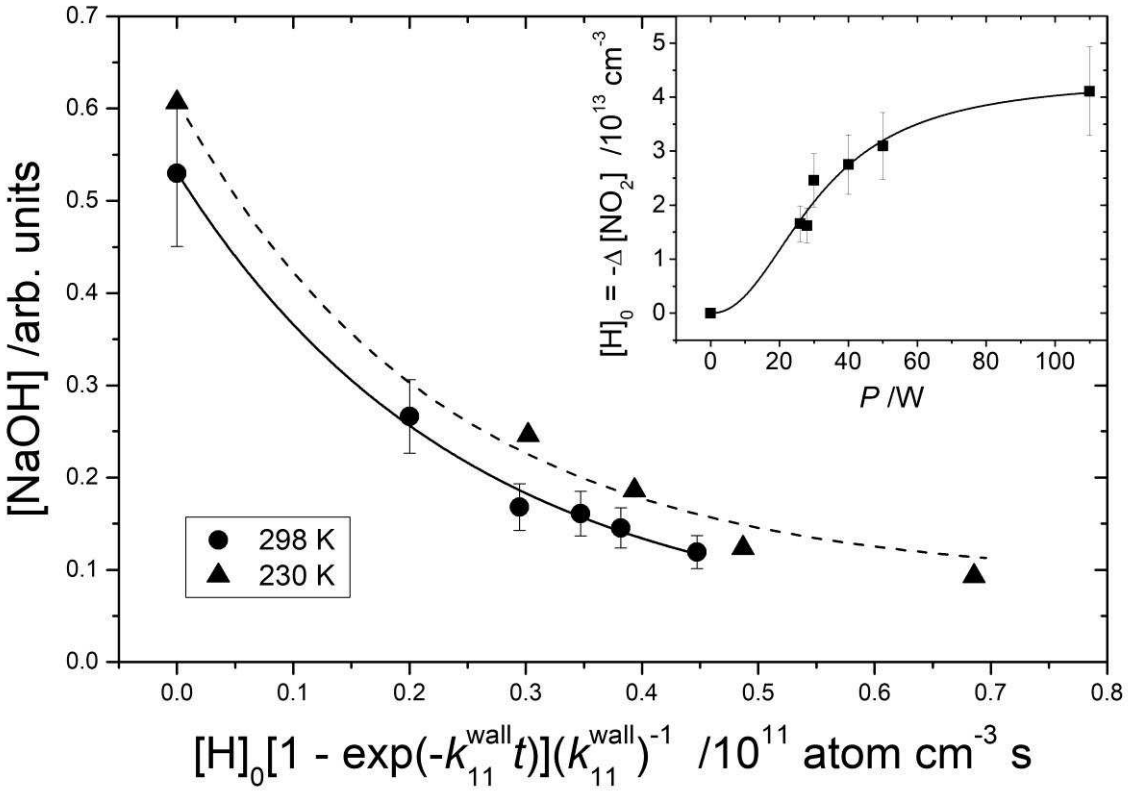

Figure 3. Decay of NaOH upon addition of H as measured with the PI-ToF-MS system at 298 K (circles) and 230 K (triangles). Exponential decay fits of the experimental data are also shown (solid and dashed lines). [NaOH] is plotted against $[H]_0\left[1 - \exp\left(- k_{11}^{wall} t\right)\right] \left(k_{11}^{wall}\right)^{-1}$ (following E4) to account for the different contact time and wall loss rate at different temperatures. The insert shows the correspondence between the H atom concentration at the injection point ($[H]_0$) and MW discharge power (P, in Watts).

Figure 4

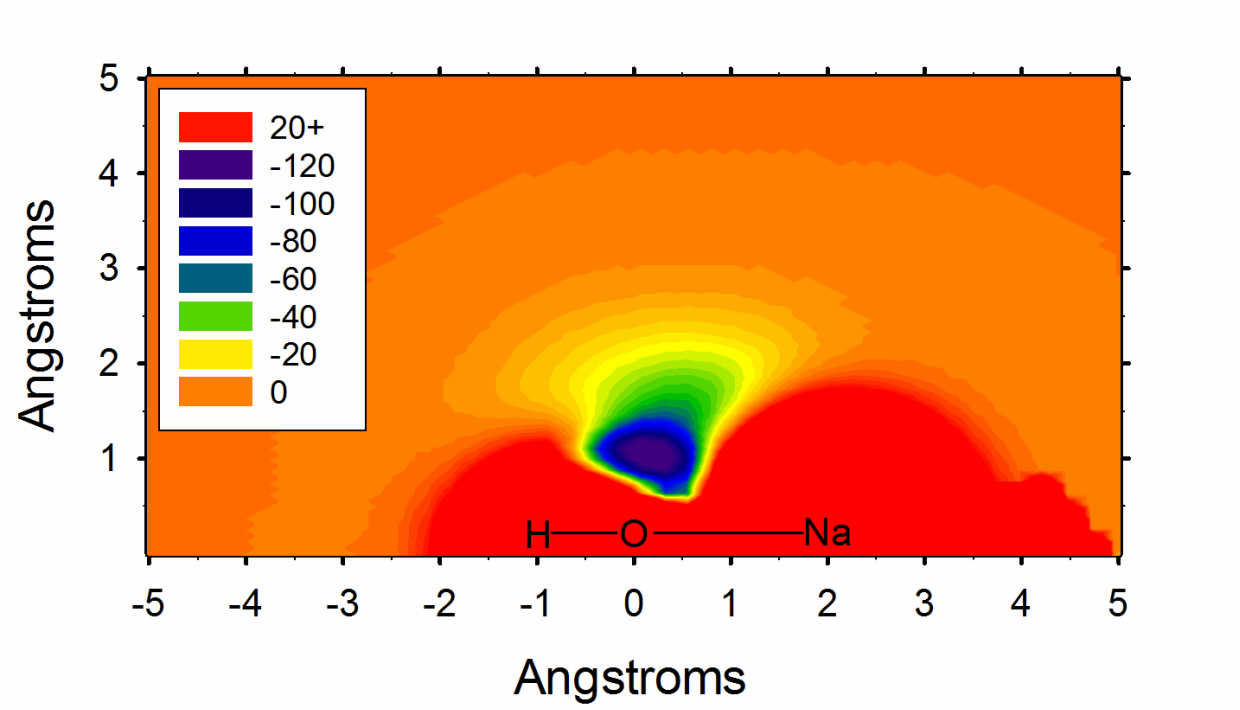

Figure 4. Potential energy surface (units: kJ mol^{-1}) for coplanar collisions of NaOH (frozen geometry) and H, calculated at the MP2/6-311+G(2d,p) level of theory.

Figure 5

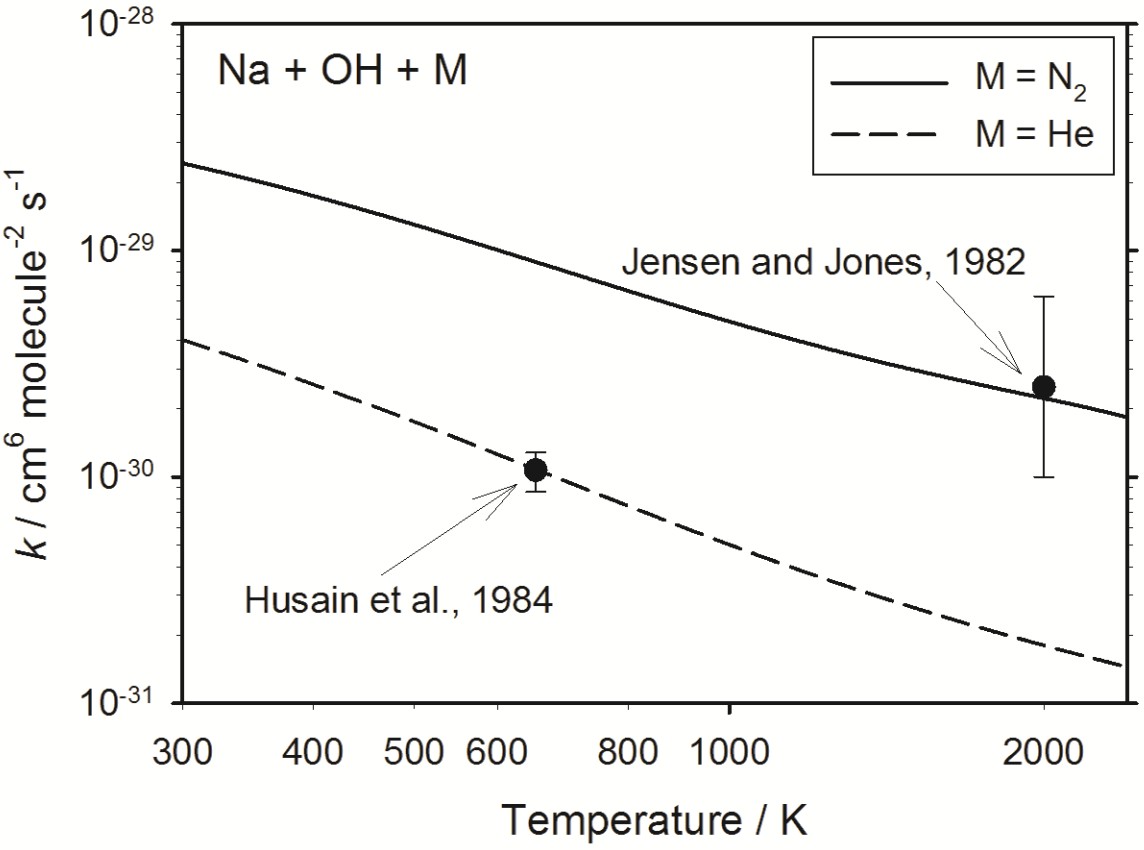

Figure 5. Calculated values of k_6(Na + OH + M) as a function of temperature for M = N_2 and He, compared with measurements in He [23] and N_2 [19].

TOC Graphic

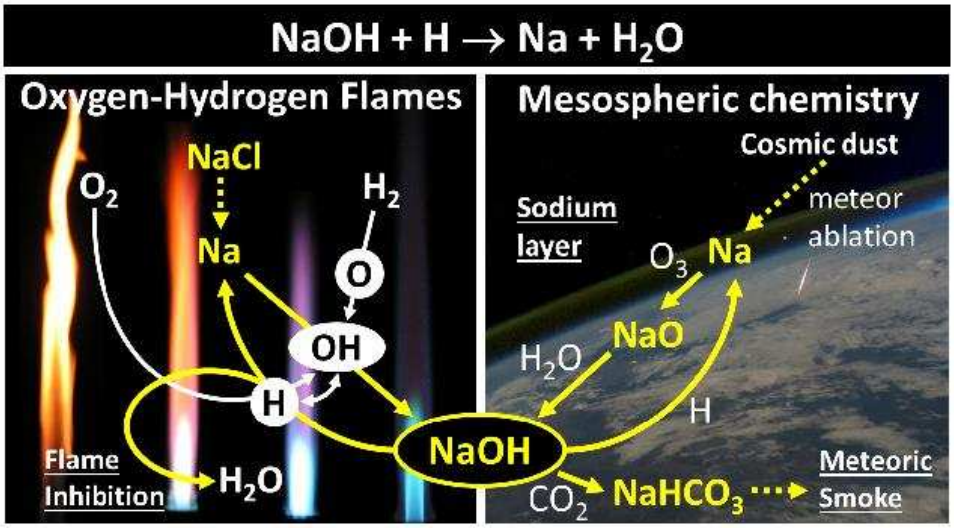
NaOH + H → Na + H2O
Oxygen-Hydrogen Flames
Mesospheric chemistry
NaCl
O2
H2
Na
O
OH
H
Flame
Inhibition
H2O
NaOH
Cosmic dust
meteor
ablation
Sodium
layer
O3
Na
NaO
H2O
H
CO2
NaHCO3
Meteoric
Smoke